Materials Transactions, Vol. 54, No. 6 (2013) pp. 872 to 878
Special Issue on Nanojoining and Microjoining
©2013 The Japan Institute of Metals and Materials

Mechanism of Low Temperature Sintering-Bonding through *In-Situ* Formation of Silver Nanoparticles Using Silver Oxide Microparticles

Fengwen Mu[1,2,*], Zhenyu Zhao[1,2,*], Guisheng Zou[1,2], Hailin Bai[1,2], Aiping Wu[1,2], Lei Liu[1,2], Dongyue Zhang[1,2] and Y. Norman Zhou[1,2,3]

[1]*Department of Mechanical Engineering, Tsinghua University, Beijing 100084, P. R. China*
[2]*Key Laboratory for Advanced Materials Processing Technology, Ministry of Education, China*
[3]*Department of Mechanical and Mechatronics Engineering, University of Waterloo, 200 University Avenue West, Waterloo, ON, N2L 3G1, Canada*

In this paper, a low temperature sintering-bonding process through *in-situ* formation of silver (Ag) nanoparticles using silver–oxide (Ag_2O) microparticles was studied. The Ag_2O powders were mixed with triethylene glycol (TEG) to form a paste, which was used to bond the Ag-coated copper (Cu) bulks. The results revealed that high temperature was helpful to increase the bond strength, and the joints average shear strength can reach 21.9 MPa at 523 K under 2 MPa for 5 min. And the mechanism of the reaction and sintering bonding process were basically made clear by using TGA-FTIR, FE-SEM and XRD, further, a reasonable sintering-bonding model was proposed. [doi:10.2320/matertrans.MD201231]

(Received December 17, 2012; Accepted March 25, 2013; Published May 25, 2013)

Keywords: *silver oxide, sintering-bonding, in-situ formation, mechanism*

1. Introduction

In microelectronic industries, Pb-containing solder is used widely for its characteristics such as ease of handing, good wettability and low cost. Whereas, due to Pb's toxicity, the use of Pb-containing solders raised a serious environmental concern and was banned by the European Restriction of Hazardous Substances (RoHS) directives. Numerous Pb-free alternatives have been studied.[1,2] The eutectic Sn–Pb alloy (melting point 456 K) has already been replaced by the Sn–Ag–Cu alloys. However, there are no suitable Pb-free high temperature solders (melting point >523 K) except candidates such as Au–Sn, Zr–Sn and Bi-based alloys. In the case of the lack of suitable non-Pb alternatives, European RoHS regulations temporarily exempt high-Pb solders used as component solders and die attachment for automotive and other high temperature applications.[3,4] It is necessary to find Pb-free alternatives for high temperature applications.

In recent years, a low temperature bonding process by means of nanojoining technology gives us a potential method to seek for suitable Pb-free packaging technology.[5] Bulk Ag has good properties such as high electrical and thermal conductivity and limited fatigue. These good properties as well as its high melting point (1233 K) make Ag a suitable material for high-temperature packaging applications.[3] And since Ag nanoparticles have low sintering temperature resulted from the high surface energy, Ag nanojoining allows a low temperature process, which can serve in a higher temperature environment.[6,7] E. Ide *et al.*, have published a bonding process using Ag nanoparticle paste which was prepared by mixing an organic solvent with Ag nanoparticles at a temperature of 573 K.[8] Lu's group has investigated the bonding of large-area (>100 mm^2) chips at about 548 K under 1–5 MPa using Ag nanoparticle paste, which was prepared by mixing various organic components (including dispersant/surfactant, binder and thinner) and chemically-reduced Ag nanoparticles.[9] Hu's *et al.*, have confirmed that the sintered network of Ag nanoparticles can work as bonding structures for Cu wires at as low as temperature of only 373 K.[10]

Only considering the performance, Ag nanoparticle paste is expected to be widely used in Pb-free high temperature application, but there still exist some problems. The main problem is the preparation of Ag nanopartciles, which is complicated, low-output and expensive. So developing a simple and low-cost Ag nanojoining is necessary.

It is well known that Ag_2O microparticles is obviously cheap and can be reduced to Ag just simply heated in air. Furthermore, if the Ag reduced from Ag_2O microparticles is in nanometer scale, Ag_2O microparticles have the potential to be a bonding material used in Pb-free high temperature application.

Recently, a novel bonding process through *in-situ* formation of Ag nanoparticles using Ag_2O microparticles has been proposed. Hirose *et al.*, got Ag nanoparticles in bonding process by reducing Ag_2O microparticles using triethylene glycol (TEG) or myristyl alcohol, which is easy to operate and low cost. They have confirmed the bonding capability, the state changes of Ag_2O particles during reduction, and the condition of the interfacial bonding utilizing Ag_2O-derived Ag nanoparticles using SEM, TEM observation as well as molecular dynamics simulation.[11–13] However, the mechanisms of reaction and sintering bonding process are still not very clear.

In this paper, the mechanism of the reaction and sintering bonding process were basically made clear by using TGA-FTIR, FE-SEM and XRD. Additionally, a sintering-bonding model was proposed through the analysis on the appearance changes from Ag_2O microparticles to Ag nanoparticles and the microstructure of the joint interface.

*Graduate Student, Tsinghua University

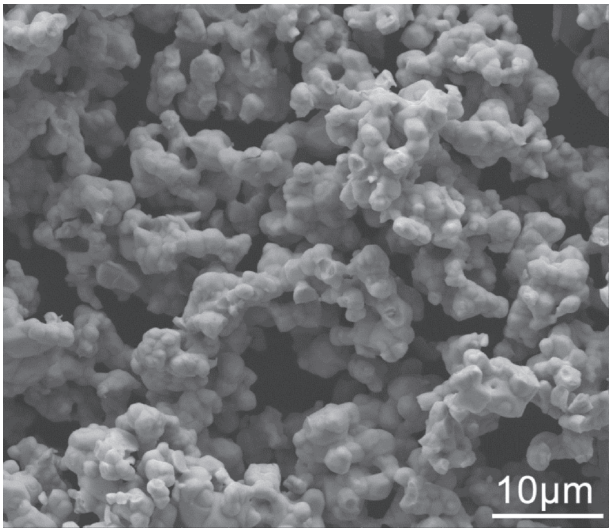

Fig. 1 SEM image of Ag_2O microparticles.

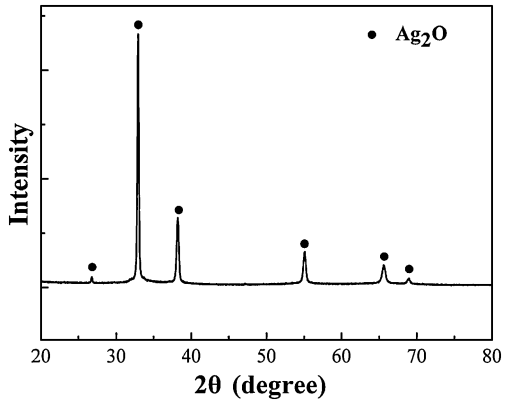

Fig. 2 XRD result of the micro-scale Ag_2O powders.

2. Experimental Details

2.1 Experimental materials

Commercially Ag_2O microparticles used in this study was shown in Fig. 1. The Ag_2O powders were tested by using the X-ray diffraction. The XRD result is showed in Fig. 2, which indicates that there is only Ag_2O powders. A paste was prepared by mixing the Ag_2O powders and commercial TEG. Figure 3 showed the schematic diagram of the assembly of Cu bulks and the shear test method. The material of the specimen is Cu. On the surface of Cu cylinders, 4 μm-thick Ag plating was applied over the 2 μm-thick nickel plating layer.

2.2 Mechanism of the reaction and sintering bonding process

In order to clearly figure out the reaction and sintering bonding process, the phase changes from micro-Ag_2O particles to Ag nanoparticles and the products from the reduction reaction in the paste were both studied.

2.2.1 Observation of the phase changes from micro-Ag_2O particles to Ag nanoparticles

After coating the Ag_2O-TEG paste on the plated Cu cylinders, the ready-made samples were cooled at room temperature after heated to different temperature (413 K, 433 K, 453 K, 473 K, 523 K, 573 K) at a heating rate of 10 K/min in air. Then the states of Ag_2O particles were observed. The reduction of Ag_2O and the behavior of the Ag nanoparticles after the reduction were analyzed. In addition, the phase change was verified by X-ray diffraction (XRD) analysis using a Bruker D8-ADVANCE X-ray diffractometer with a Cu–Kα Radiation ($\lambda = 0.15418$ nm) at 40 kV and 40 mA.

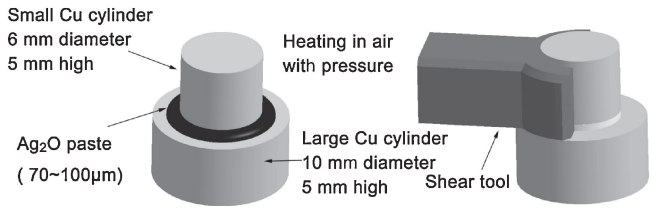

Fig. 3 Schematic diagram of the assembly of Cu bulks and shear teat method.

2.2.2 Confirmation of products from the reduction reaction in Ag_2O-TEG paste

To investigate the reaction process, Thermogravimetry coupled to Fourier transform infrared spectroscopy (TGA-FTIR) was used to study reaction products of the paste heated in air and nitrogen respectively. The thermogravimetric/differential thermal analysis was performed using a NETZSCH STA 409C/3/F at the temperature range of 323 to 773 K with a heating rate of 10 K/min. FTIR spectras were recorded on a Nicolet-Nexus 670 FTIR spectrometer with a deuterated triglycine sulfate detector (DTGS). The FTIR spectras were recorded in the spectral range of 4000–400 cm^{-1} with a 4 cm^{-1} resolution and averaging 32 scans. In spectras, one product had its special wave bands, and through the absorbance change of a same product, the quantity of the products can be reflected.

2.3 Evaluation of bonding conditions

In the assembly of Cu bulks, the micro-Ag_2O paste was coated on the faying surfaces about 70–100 μm in thickness. In order to investigate the effects of holding temperature, the assembled bulks were heated up to different temperature (453 K, 473 K, 523 K, 573 K, 623 K) at the rate of 10 K/min in air under pressure of 2 MPa. Shear strength of the joints was used to evaluate the joints strength. The joint shear strength was measured using the Thermal-Mechanical Simulator Gleeble 1500D with 5 mm/min displacement rate at room temperature. The joint cross-sections were observed by FE-SEM (FEI Quanta 200 FEG). The cross-section samples were prepared by grinding, polishing and eroding. The corrosive solution was the mixture of ammonia water and hydrogen peroxide of which the concentration is 30%.

3. Results and Discussion

3.1 Transformation of the Ag nanoparticles from micro-Ag_2O and their sintering behavior

Microstructures of the micro-Ag_2O pastes heated at different temperature were shown in Fig. 4. From Figs. 4(a), 4(b) and 4(c), it can be seen that the amount and size

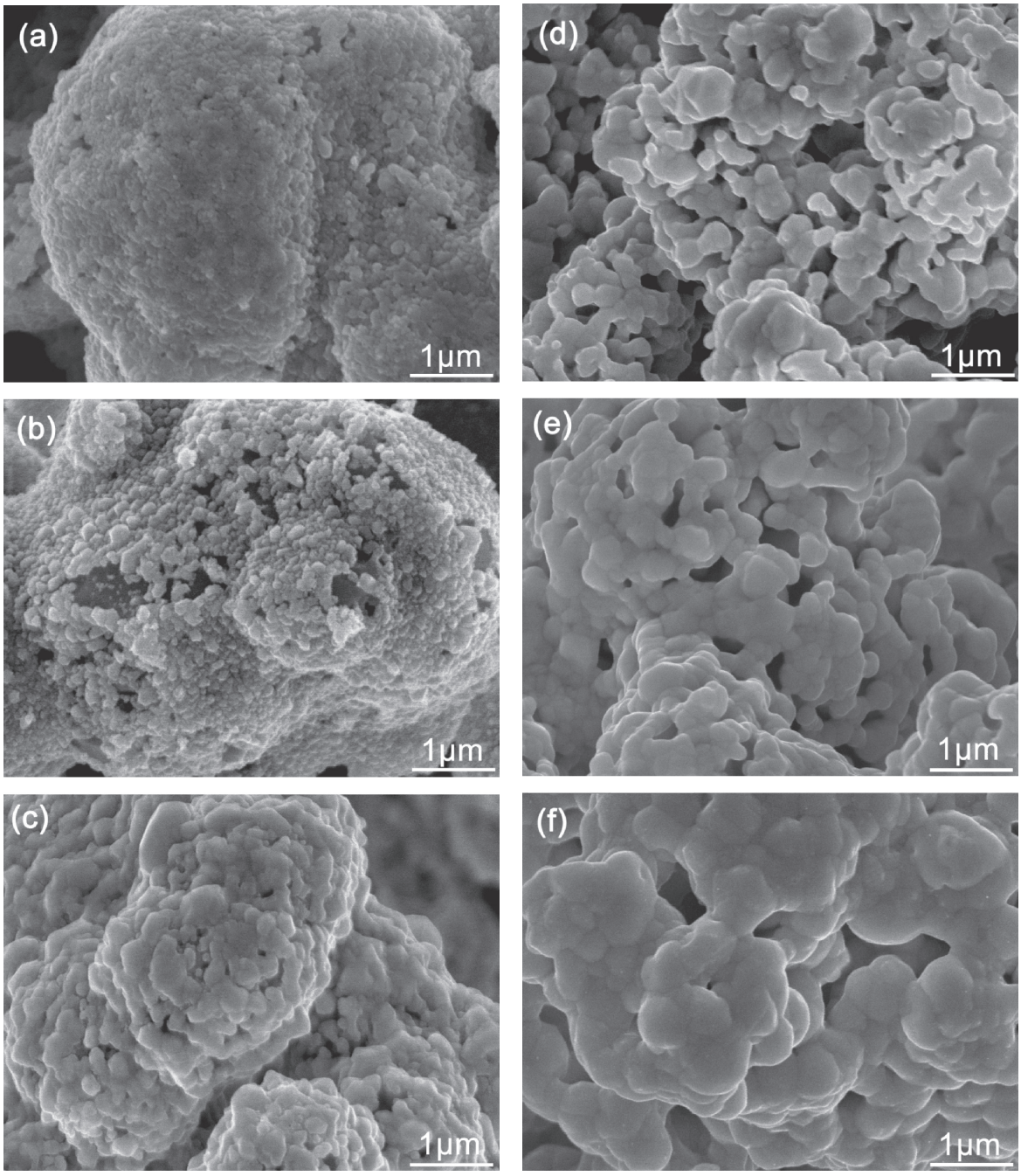

Fig. 4 Microstructures of the micro-Ag_2O pastes heated to different temperature (a) 413 K, (b) 433 K, (c) 453 K, (d) 473 K, (e) 523 K, (f) 573 K.

of nanoparticles transformed from Ag_2O increase with the rise of temperature from 413 to 453 K. Correspondingly, XRD result of the micro-Ag_2O pastes heated at 413, 433 and 453 K was shown in Fig. 5. In Fig. 5, the strength value of Ag and Ag_2O peaks increase and decease respectively with heating temperature rising from 413 to 453 K. It is visible that when the paste was heated up to 413 K, only a bit of Ag_2O particles decomposed into Ag and, while, when the temperature was up to 453 K, the Ag_2O almost ran out into Ag nanoparticles. So it can be demonstrated that in Fig. 4(a), the nanoparticles distributed on the surface of micro-Ag_2O particles was Ag nanoparticles and when the temperature was 453 K, almost all the Ag_2O particles were transformed into Ag nanoparticles, as shown in the Fig. 4(c). Furthermore, according to Figs. 4(a), 4(b) and 4(c), it can be inferred that Ag atoms were first reduced from the surface of micro-Ag_2O particle, then inward until the whole Ag_2O particle transformed into Ag. And these formed Ag atoms were immediately aggregated into Ag nanoparticles which were absorbed to the Ag_2O particles. Moreover, we think that the reaction and aggregation processes are almost simultaneous. The viewpoint just mentioned above can be partly proved by the interface microstructure of the joints, which would be discussed in the following section.

Moreover, in Figs. 4(c), 4(d), 4(e) and 4(f), with temperature rising from 453 to 573 K, the amount of nanoparticles decreased and the density of the microstructures increased.

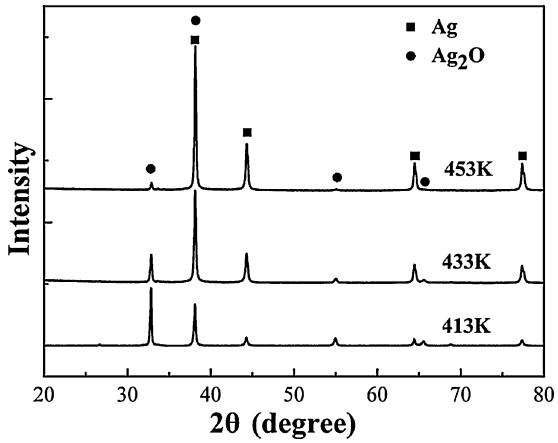

Fig. 5 XRD results of the micro-Ag_2O paste heated to different temperature without holding (a) 413 K, (b) 433 K, (c) 453 K.

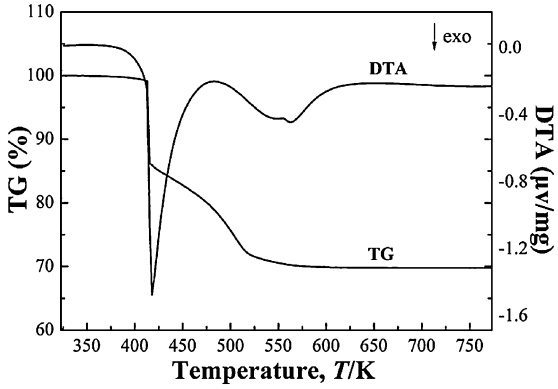

Fig. 6 TG-DTA curves of the micro-Ag_2O paste heated in air.

3.2 Equation of the reaction happened in the Ag_2O paste when heated and explanation of the whole reaction process

Figure 6 showed the TG-DTA curves of the paste heated in air. It can be seen that both DTA curve and TG curve of the paste fell sharply at around 418 K. In Fig. 6, besides the descent stage of the TG-DTA curves at about 418 K, the other exothermal peak was also found in the section of the DTA curve between 473 and 623 K. Correspondingly, the TG curve showed the weight loss in the section from 473 to 623 K.

Figure 7 showed the FTIR spectras of the gaseous products generated from micro-Ag_2O paste heated in air. When the heating temperature was 373 K, there only existed the bands of carbon dioxide (2391–2217, 726–586 cm^{-1}) and water (3964–3038, 1300–1800 cm^{-1}). This is the measurement background. When the temperature was up to 418 K, no other things bands occurred, yet the absorbance of CO_2 and H_2O increased very sharply (Since the quantity change of CO_2 and H_2O was consistent, we just studied the change of CO_2 quantity in the following sections). When the temperature was up to 468 K, the bands at 3000–2650 cm^{-1} for the C–H and CH_2 stretching vibration, the bands at 1850–1600 cm^{-1} for the C=O double bond stretching vibration and the bands at 1500–900 cm^{-1} for C–H in-plane bending vibration, C–O skeleton vibration and C–C skeleton

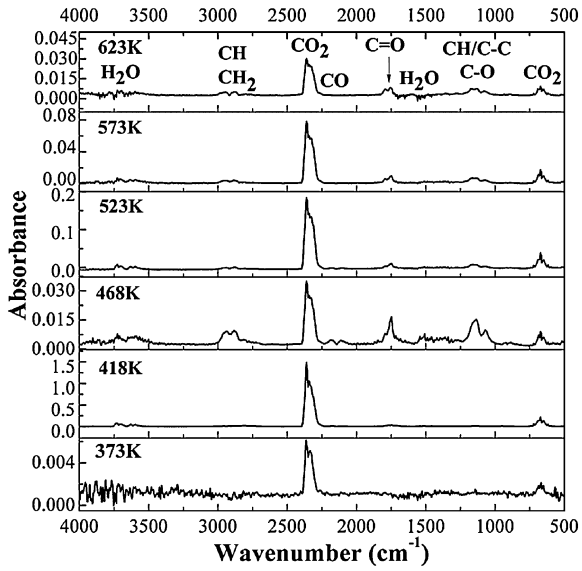

Fig. 7 FTIR spectras of gaseous products generated from micro-Ag_2O paste heated to different temperature in air.

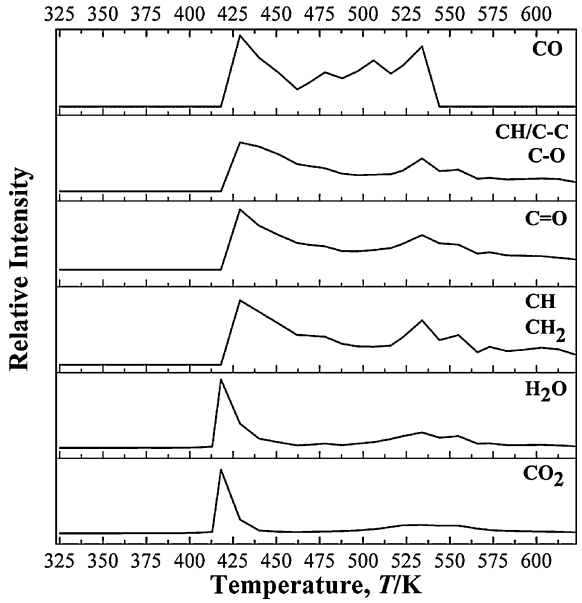

Fig. 8 Absorbance of gaseous products generated from micro-Ag_2O paste with the increase of heating temperature in air.

vibration appeared; these bands were corresponded to the things such as alkanes, aldehydes, ketones, carboxylic acids and alcohols; moreover, relatively weaker bands of the carbon monoxide (2180–2112 cm^{-1}) also occurred at 468 K. However, the absorbance of CO_2 decreased a lot. When the temperature increased up to 523 K, the absorbance of CO_2 increased once again. From 573 and 623 K, it can be seen that the absorbance of CO_2 decreased with the increasing of temperature.

Figure 8 showed the relationship between the temperature and the absorbance of gaseous products generated from micro-Ag_2O paste heated in air, which represented the change of the gaseous products quantity. As mentioned above, the amount of CO_2 appeared two peaks respectively at 418 and 523 K. Combined with the TG-DTA curves of the micro-

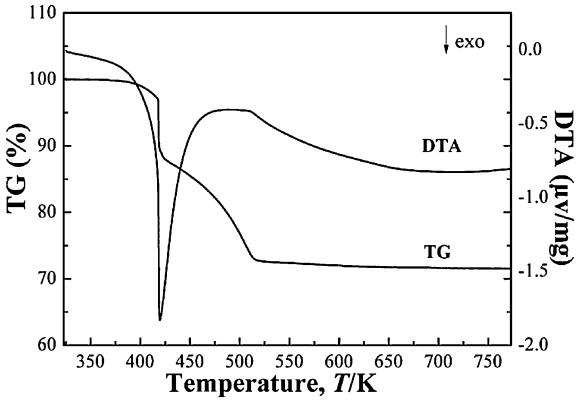

Fig. 9 TG-DTA curves of the micro-Ag_2O paste heated in nitrogen.

Ag_2O paste heated in air, it can be seen that the two exothermal peaks in Fig. 6 were responded to the absorbance peaks of CO_2 in Fig. 8. At about 418 K, we can get that the gaseous product was mainly CO_2 and H_2O. From 429 K, there were by-products generated from the oxidation of TEG by oxygen (O_2), which could be seen when the amount of CO_2 decreased; at around 523 K, the second absorbance peaks of CO_2 can be explained by the reaction between the by-product and O_2, which also caused the second exothermal peak.

Figure 9 showed the TG-DTA curves of the micro-Ag_2O paste heated in nitrogen. An exothermal peak was detected at around 418 K in the DTA curve, and simultaneously a great weight loss occurred in the TG curve. However, compared with 15% of weight loss in the TG curve shown in Fig. 6, the percent of the paste weight loss in Fig. 9 was just 10%. The difference was thought to be caused by the presence of O_2 or not. So we can ascertain that at about 418 K, there exist reactions between the TEG and O_2. After about 513 K, there was a process of releasing heat slowly, which was also different with the DTA curve obtained in air. This was considered that there only existed the slowly self-decomposition of the residual TEG for the shortage of O_2.

Figure 10 showed the FTIR spectras of the gaseous products generated from micro-Ag_2O paste heated in nitrogen. When the temperature was 373 K, there was only very little CO_2 and H_2O. At 418 K, the quantity of CO_2 increased very much and no other bands of by-products occurred. When the temperature was 468 K, the quantity of CO_2 decreased and the bands of by-products could be seen. From 468 to 623 K, it can be ascertained that the quantity of CO_2 increased slowly with the temperature and the absorbance change of the by-products was small.

Figure 11 gave the absorbance of gaseous products generated from micro-Ag_2O paste with the increase of heating temperature in nitrogen, which represented the variation of gaseous products quantity with the increasing of heating temperature. At about 418 K, we can also get that the gaseous product was mainly CO_2 and H_2O; from 429 K, little by-products might be generated from self-decomposition under heating in nitrogen.

Considering the measurements in air and in nitrogen together, we can figure out the TG-DTA curves in air. At

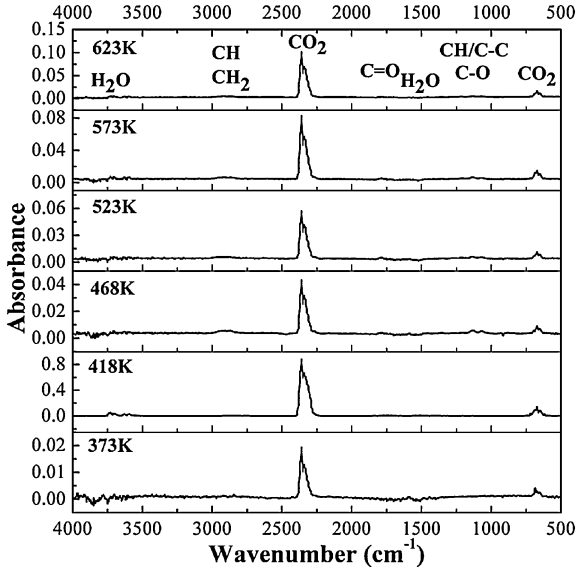

Fig. 10 FTIR spectras of gaseous products generated from micro-Ag_2O paste heated in nitrogen.

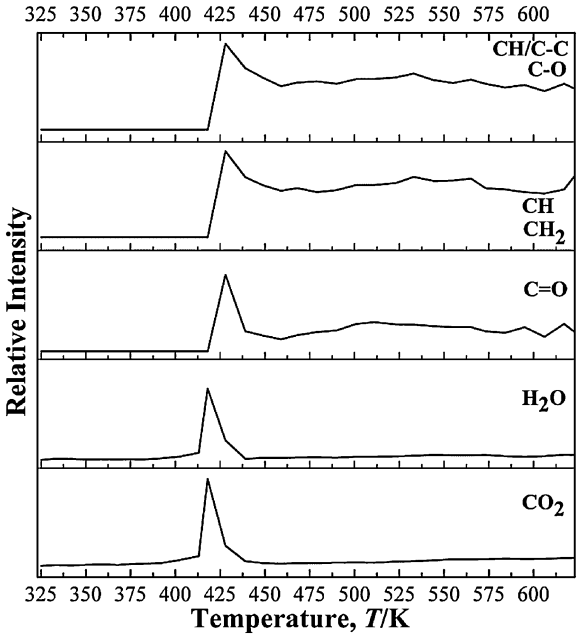

Fig. 11 Absorbance of gaseous products generated from micro-Ag_2O paste with the increase of heating temperature in nitrogen.

about 418 K, there existed an intensely reaction. The main reaction was the reduction reaction of Ag_2O. The reaction equation was thought to be

$$Ag_2O + C_6H_{14}O_4 \xrightarrow{418K} Ag + CO_2\uparrow + H_2O\uparrow$$

Meanwhile, there also were some by-reactions, which were the oxidation of TEG by O_2. The section of the TG-DTA curves from 418 to 623 K was thought to be an evaporation, self-decomposition and oxidative-decomposition process of the residual TEG and the by-products. After 473 K, the heat released from the decomposition process was more than the heat absorbed for evaporation, so the other exothermal peak occurred in the DTA curve obtained in air.

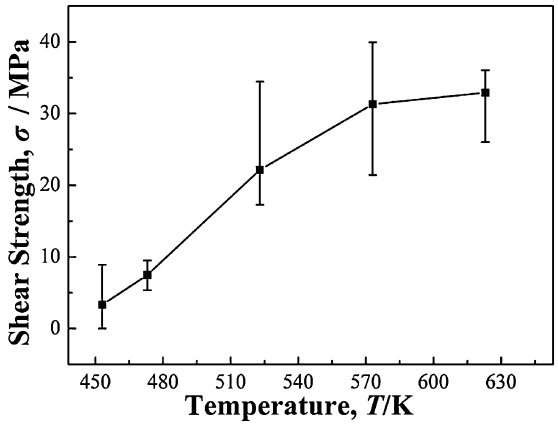

Fig. 12 Relationship between the joint strength and bonding temperature.

There is a difference of completed temperature about the transformation from micro-Ag_2O particles to Ag nanoparticles between the TG-DTA result and XRD result, which was caused by the sample quantity. The XRD analysis needed much more sample than the TG-DTA analysis, which just needed about 70–100 mg. The heat transmission process in the XRD analysis sample when heated resulted in the higher completed temperature of the transformation.

3.3 Performance of the joint obtained at different temperature

The relationship between the joint strength and bonding temperature was shown in Fig. 12. The joint was obtained in air at an applied pressure of 2 MPa and a given heating temperature for 5 min. It could be seen that high temperature was helpful to increase the bond strength, and the average shear strength can reach 21.9 MPa at 523 K. When the temperature was exceeded 573 K, the increase of the joint strength was not very obvious.

Figure 13 showed that the cross-sectional SEM images of joints made at 523 K, 573 K. In Fig. 13, it can be seen that the density of the porous sintered layer increased with the increasing of temperature. Moreover, there existed some no-bonding zones at the interface between the sintered layer and the coated Ag layer. That is to say, the Ag atoms reduced from the micro-Ag_2O particle surface didn't spread out on the coated Ag layer. So, combined with the Figs. 4(a), 4(b) and 4(c), we thought that the reduction product Ag atoms were first reduced from the surface of micro-Ag_2O particle but gathered to be Ag nanoparticles on the surface of micro-Ag_2O particle instantaneously, then inward until the whole Ag_2O particle transformed into Ag. Finally, the Ag nanoparticles were sintered and bonded with each other. The model scheme of the reaction and bonding mechanism was shown in the Fig. 14.

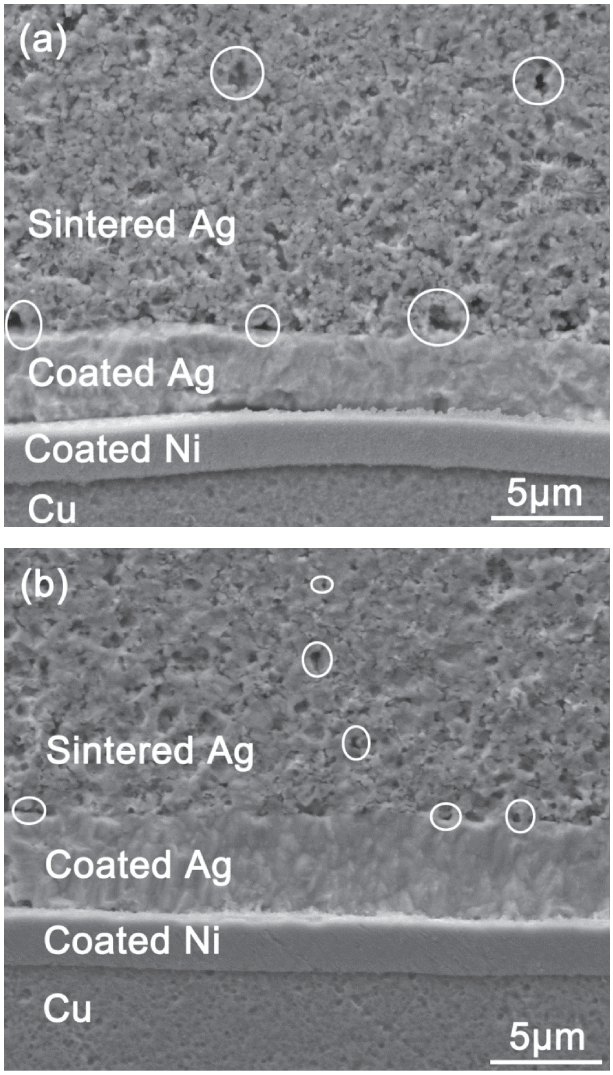

Fig. 13 Cross-sectional SEM images of joints made at different temperature with a pressure of 2 MPa and a holding time of 5 min: (a) 523 K, (b) 573 K.

4. Conclusion

The mechanism of low temperature sintering-bonding through *in-situ* formation of Ag nanoparticles using micro-Ag_2O particles was studied. Firstly, the process of the phase changes from micro-Ag_2O particles to Ag nanoparticles and the XRD result of the micro-Ag_2O pastes heated at 413 K, 433 K, 453 K were analyzed. Secondly, the reaction process was investigated using the Thermogravimetry coupled to Fourier transform infrared spectroscopy (TGA-FTIR). Lastly, the effects of bonding temperature on the shear strength and the cross-section of the joints were discussed. The main conclusions were remarked as follows.

(1) Ag atoms were first reduced from the surface of micro-Ag_2O particle, then inward until the whole Ag_2O particle transformed into Ag. And these formed Ag atoms were immediately aggregated into Ag nanoparticles which were absorbed on the Ag_2O particles. This was partly proved by the microstructure of the joints cross-section.

(2) The TG-DTA curves of the paste heated in air can be explained by the reaction products, which were confirmed by the FTIR analysis. The main reaction at 418 K was the reduction reaction of Ag_2O. The reaction equation was thought to be

$$Ag_2O + C_6H_{14}O_4 \xrightarrow{418K} Ag + CO_2\uparrow + H_2O\uparrow$$

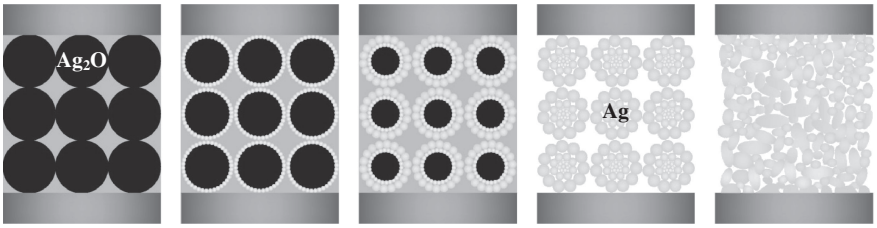

Fig. 14 Model schemes of the reaction and bonding mechanism of the low temperature sintering-bonding through *in-situ* formation of Ag nanoparticles using Ag_2O microparticles.

Meanwhile, there also were some by-reactions, which were the oxidation of TEG by O_2. The second exothermal peak was thought to be caused by the reaction between the by-product and O_2. Moreover, the section of the TG-DTA curves from 418 to 623 K was thought to be an evaporation, self-decomposition and oxidative-decomposition process of the residual TEG and the by-products.

(3) High temperature was helpful to increase the bond strength, and the average shear strength can reach 21.9 MPa at 523 K under 2 MPa for 5 min. The sintered layer was porous and the density of the sintered layer increased with the rise of temperature. In addition, there existed some no-bonding zones at the interface between the sintered layer and the coated Ag layer.

Acknowledgments

This research was supported by the National Natural Science Foundation of China (No. 51075232) and by State Key Lab of Advanced Welding & Joining, HIT (No. AWPT-Z12-04) and by Tsinghua University Initiative Scientific Research Program (No. 2010THZ 02-1).

REFERENCES

1) Y. Li, K. Moon and C. P. Wong: Science **308** (2005) 1419–1420.
2) F. P. McCluskey, M. Dash, Z. Wang and D. Huff: Microelectron. Reliab. **46** (2006) 1910–1914.
3) H. Ogura, M. Maruyama, R. Matsubayashi, T. Ogawa, S. Nakamura, T. Komatsu, H. Nagasawa, A. Ichimura and S. Isoda: J. Electron. Mater. **39** (2010) 1233–1240.
4) K. Suganuma, S. J. Kim and K. S. Kim: JOM **61** (2009) 64–71.
5) Y. Zhou: *Microjoining & Nanojoining*, (Woodhead Publishing Ltd., Cambridge, England, 2008).
6) T. Morita, E. Ide, Y. Yasuda, A. Hirose and K. Kobayashi: Jpn. J. Appl. Phys. **47** (2008) 6615–6622.
7) M. Maruyama, R. Matsubayashi, H. Iwakuro, S. Isoda and T. Komatsu: Appl. Phys. A **93** (2008) 467–470.
8) E. Ide, S. Angata, A. Hirose and K. F. Kobayashi: Acta Mater. **53** (2005) 2385–2393.
9) T. G. Lei, J. N. Calata and G. Q. Lu: IEEE Trans. Compon. Packag. Tech. **33** (2010) 98–104.
10) A. Hu, J. Y. Guo, H. Alarifi, G. Patane, Y. Zhou, G. Compagnini and C. X. Xu: Appl. Phys. Lett. **97** (2010) 153117–153117-3.
11) A. Hirose, H. Tatsumi, N. Takeda, Y. Akada, T. Ogura, E. Ide and T. Morita: J. Phys. Conf. Series (2009) p. 0127074.
12) T. Morita, Y. Yasuda, E. Ide, Y. Akada and A. Hirose: Mater. Trans. **49** (2008) 2875–2880.
13) T. Ogura, M. Nishimura, H. Tatsumi, N. Takeda, W. Takahara and A. Hirose: Open Surf. Sci. J. **3** (2011) 55–59.